

## Effect of hydrogen on vacancy diffusion

Sebastián Echeverri Restrepo <sup>\*</sup>

*SKF Research & Technology Development (RTD), SKF B.V., Meidoornkade 14, 3992 AE, Houten, The Netherlands and Department of Physics, King's College London, Strand, London WC2R 2LS, United Kingdom*

Henry Lambert  and Anthony T. Paxton 

*Department of Physics, King's College London, Strand, London WC2R 2LS, United Kingdom*



(Received 20 April 2020; accepted 19 October 2020; published 4 November 2020)

Although it is widely recognized that even small amounts of hydrogen (H) can cause embrittlement in iron (Fe) and in (high-strength) steels, the fundamental mechanisms that cause it are not yet completely understood. To contribute to a better understanding of the behavior of H in metals, we use parallel replica dynamics (PRD) to study the effect that different amounts of atomic H have in the diffusion of a single vacancy in body-centered cubic (BCC) Fe. Using PRD we calculate the diffusion of H-vacancy complexes at temperatures and timescales that are not reachable using classical methods. Additionally, based on the PRD results and calculations of the minimum energy paths of migration, we propose a mechanism for the migration of vacancy-H complexes and formulate an analytical model for the calculation of their joint diffusivity.

DOI: [10.1103/PhysRevMaterials.4.113601](https://doi.org/10.1103/PhysRevMaterials.4.113601)

### I. INTRODUCTION

Atomic hydrogen, H, can have a detrimental effect on the mechanical properties of steels. The presence of small quantities of diffusing hydrogen can reduce the toughness and breaking strain of steel, making it behave in a brittle manner [1–3]; in some applications this can lead to catastrophic failures. For instance, in the case of roller bearings considerable reductions in the fatigue life have been measured [4].

The constant industrial need for simultaneously lighter, harder, more ductile, and more resistant materials is continuously pushing the steel making industry to develop new types of high-strength steels [5,6]. One of the issues with the newest generations of steels is that the embrittling effect of hydrogen usually correlates with their strength [6]; this means that the higher the strength of the steel, the more susceptible to hydrogen embrittlement it will be.

In order to circumvent the problems caused by hydrogen, different solutions have been put forward [7–10], some more successful than others. Nevertheless, a definitive “cure” remains to be proposed. One of the reasons for the lack of satisfactory solutions is that, although much research has been done on the topic, the fundamental mechanisms of hydrogen embrittlement are still not well understood.

Due to its limited solubility in Fe at room temperature, hydrogen is known to accumulate in deformation-induced defects. In the present work we focus on the influence of atomic hydrogen in the behavior of one of the most fundamental defects in crystalline materials: vacancies [11]. Vacancies play an important role in the creep behavior of steels. We use parallel replica dynamics (PRD) and classical interatomic

potentials to study how the presence of H affects the diffusivity of vacancies at temperatures and timescales that are not reachable using classical dynamic simulation methods. We then complement the study with nudged-elastic-band calculations of the minimum energy migration paths of vacancy-H complexes using both classical potentials and quantum mechanical methods, and propose an analytical model to calculate the diffusivity of single vacancies in such systems.

The structure of the paper is as follows: We start by introducing the main methods used in the article (Sec. II), namely, the selection of the interatomic potential for the molecular dynamics (MD) and PRD simulations, and the parameters used for the calculation of the energetics using quantum mechanics. We then present results of the diffusivity and migration energies of vacancy-hydrogen complexes using classical potentials and use those results to propose a model to describe the effect of hydrogen on the diffusivity of the vacancies (Sec. III). We finally refine the predictions of the model by using more accurate migration barriers from tight-binding (TB) nudged-elastic-band (NEB) calculations (Sec. IV).

### II. METHODS

#### A. EAM: Interatomic potential

The dynamic calculations presented in this article were carried out using molecular dynamics (MD) and parallel replica dynamics (PRD) together with the the Fe-H interatomic potential originally developed in Ref. [12] (Potential B) and later modified in Ref. [13] (Parametrization B) to lessen the artificial attractive interactions between neighboring H atoms and prevent unphysical H aggregation in single-crystal Fe. This potential takes the Fe-Fe interactions from Ref. [14] and was built within the framework of the embedded atom method

<sup>\*</sup>sebastianecheverri@gmail.com

TABLE I. Change in energy  $\delta E$  required to trap an additional hydrogen (H) atom inside a Fe vacancy (Va). The results were obtained using molecular statics. For comparison, results using classical and quantum mechanical models from the literature are also presented. In all cases, the six available tetrahedral sites are initially occupied in the same order as in Refs. [12,13,19,20].

	$\delta E$ [eV]				
	EAM	EAM [13]	DFT [19]	DFT [20]	TB [21]
VaH	0.603	0.603	0.559	0.60	0.319
VaH <sub>2</sub>	0.552	0.552	0.612	0.61	0.330
VaH <sub>3</sub>	0.298	0.298	0.399	0.39	0.263
VaH <sub>4</sub>	0.182	-0.063	0.276	0.37	0.160
VaH <sub>5</sub>	0.056	0.263	0.335	0.31	0.144
VaH <sub>6</sub>	0.066	0.104	-0.019	-	-0.033

(EAM) formalism [15]. The selection of the potential for the present work was made based on its capability to properly simulate (1) self-diffusion processes in bulk Fe, (2) the diffusion of H in Fe, and (3) the interaction of Fe and (several) H atoms in the bulk and inside vacancies.

The Fe-Fe part of the potential was fitted to the relaxed vacancy formation and migration energies obtained from density functional theory (DFT) calculations (1.72 eV vs 1.95 eV [16] and 0.64 eV vs 0.64 eV [16], respectively). The sum of these two quantities represents the activation energy for self-diffusion and the selected potential gives a value within 10% of experimental measurements [17]. Additionally, the self-diffusivity given by the potential is in good agreement with experimental data for pure iron [18].

The Fe-H and H-H parts of the potential were fitted [12] to the strain-dependent dissolution and diffusion barriers and give a reasonable agreement with DFT calculations. Individual H atoms in tetrahedral sites and at saddle points between tetrahedral sites and H atoms bound at vacancies and at saddle points between vacancy binding sites were also used in the fitting of the parameters of the interatomic potential. The potential correctly predicts that H preferentially dissolves in the tetrahedral sites in Fe.

In order to verify the fidelity of the Va-H interactions, we calculate the change in energy  $\delta E$  required to trap an additional H atom at a single vacancy in a periodic computational “supercell” containing  $m$  Fe atoms, referenced to the bulk dissolution energy:

$$\delta E = [E(\text{Fe}_m\text{H}) - E(\text{Fe}_m)] - [E(\text{Fe}_{m-1}\text{H}_n) - E(\text{Fe}_{m-1}\text{H}_{n-1})]. \quad (1)$$

For the calculation of the change in energy  $\delta E$  we use a  $10 \times 10 \times 10$  Fe supercell and remove one Fe atom to create a vacancy. The H atoms are initially inserted into the vacancy in the same positions and order as in Refs. [12,13,19,20]. The calculated values of  $\delta E$  are presented in Table I together with other MD and DFT results from the literature. The TB energies are less than 50% underestimated with respect to the reference DFT results, and the trends are in good accord [21].

For the case of four, five, and six H atoms, the energies calculated in Ref. [13], using the same interatomic potential, are higher than the ones that we obtain. We have found using

a range of minimisers in molecular statics that the energies calculated in their work are metastable and do not correspond to minimum energy configurations. A possible explanation is that according to our results, for the interatomic potential under consideration, in the minimum energy configurations the H atoms are shifted from the octahedral sites. Note that, although the initial configurations for the various methods presented in Table I are the same, the configurations after minimization might be slightly different. There is no guarantee that they are not in a metastable state.

With respect to the quality of the predictions of  $\delta E$  of H atoms inside a vacancy, we notice that for more than three H atoms the errors start becoming considerable, e.g., -0.063 eV versus 0.276 eV [19] (0.37 eV [20]) for four H atoms. Due to magnitude of such differences, we limit the dynamic calculations to three H atoms.

### B. Energetics from quantum mechanics

The tight-binding (TB) method is the first of two quantum mechanical approaches for studying the energetics of the Fe-H vacancy migration discussed in this work. The TB model employed is the nonorthogonal *s-d* model described in Ref. [21]. This model incorporates magnetic and on-site electronic contributions to the total energy self-consistently according to the procedure described in Ref. [22]. The calculations are performed using an interface between the tbe [23] and i-pi software packages [24].

Density functional theory (DFT) calculations have also been performed for the process of vacancy diffusion. The DFT calculations were performed using the VASP package [25]. The PBE functional [26] was used to approximate the electronic exchange and correlation energy, and projector augmented wave pseudopotentials [27] were used to treat the valence electron-ion interaction. A  $4 \times 4 \times 4$  k-point mesh was used for all the configurations, and a 30 Ry energy cutoff on the plane wave expansion of the wave functions was used.

The DFT calculations provide a baseline accuracy against which the embedded atom and TB predictions for the energetics and forces may be compared. We discuss the important variations in the features of the energy pathways computed using the different potentials in Sec. III B.

### C. Parallel Replica Dynamics (PRD)

Parallel replica dynamics (PRD) [28] is a method suitable for the simulation of infrequent-event systems that obey first-order kinetics (there is an exponential distribution of first-escape times). It allows longer timescales to be reached than classical molecular dynamics (MD) by parallelizing in the time domain.

The PRD algorithm works in the following manner: First, an initial system is generated and replicated  $M$  times, that is,  $M$  exact replicas of the system are created. Second, the momenta are randomized by choosing a random set of velocities for the atoms of each replica. Third, classical MD is run on each replica for a short time ( $\tau_{\text{dephase}}$ ) to dephase the replicas and eliminate any possible correlation between them. Steps 2 and 3 are repeated  $n_{\text{dephase}}$  times. Fourth, dynamics are run continuously in each replica until an event occurs in any of

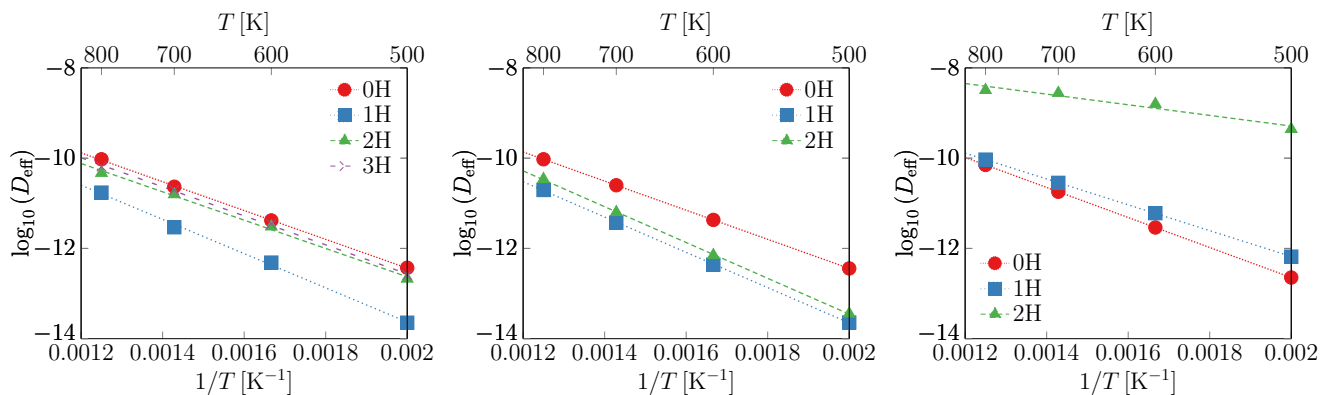


FIG. 1. Arrhenius plot of the effective diffusivities ( $D_{\text{eff}}$ ) calculated using PRD (left), our proposed model with EAM energies (center), and our proposed model with TB energies (right) for a system containing a single Fe vacancy and up to three H atoms. The units of  $D_{\text{eff}}$  are  $\text{m}^2\text{s}^{-1}$ .

them; to check for the occurrence of an event, the replicas are quenched via a conjugate gradient minimization, and the positions of the particles are compared to those in the initial system. Here we define an event as a single hop of a vacancy, in other words, as the displacement of a single Fe atom to fill a vacancy that is immediately adjacent to it. Fifth, MD is continued for a time ( $\tau_{\text{corr}}$ ) on the replica where a transition occurred to allow correlated dynamical events. Finally, the new state is replicated and the procedure is restarted. For completeness, only a brief introduction to PRD is given here. Thorough descriptions of the method are available in the literature [28,29]. We use the implementation of PRD available in the software LAMMPS [30,31].

Depending on the specific problem, the following parameters need to be selected to run PRD: (1)  $n_{\text{replica}}$ , the number of replicas; (2)  $t_{\text{total}}$ , the total simulation time, in time units (corresponding roughly to the sum of the times spent on each replica); (3)  $\tau_{\text{event}}$ , the number of time steps between event checks; (4)  $n_{\text{dephase}}$ , the number of times (stages) that each replica is run independently during dephasing; (5)  $\tau_{\text{dephase}}$ , the duration, in time steps, of each of the dephasing stages; and (6)  $\tau_{\text{correlate}}$ , after an event is detected, the number of time steps to consider correlation between events. The values of these parameters used in the current work are presented in Table II.

TABLE II. Parameters used for the PRD simulations as a function of the temperature. The same values are used for all the H concentrations. The units of  $\tau$  are time steps (the values between parentheses are written in units of ps). We use a time step of  $1.0 \times 10^{-3}$  ps.

	Temperature [K]			
	500	600	700	800
$n_{\text{replica}}$	24	12	12	12
$t_{\text{total}}$ [ $\mu\text{s}$ ]	20.0	5.0	1.5	0.2
$\tau_{\text{event}}$	100(0.1)	100(0.1)	100(0.1)	100(0.1)
$n_{\text{dephase}}$	5	5	5	5
$\tau_{\text{dephase}}$	10 000(10)	10 000(10)	10 000(10)	10 000(10)
$\tau_{\text{correlate}}$	10 000(10)	10 000(10)	10 000(10)	10 000(10)

One additional parameter that needs to be defined is  $d_{\text{event}}$ ; it corresponds to the minimum distance that an atom needs to move for it to be considered as an event. Since we are interested in vacancy diffusion, we set this value to  $1.855 \text{ \AA}$ , which corresponds to  $3/4$  of the nearest-neighbor (NN) distance. The reason for choosing this value is that the distance that an Fe atom needs to move in order to fill an adjacent vacancy is the NN distance.

Note that although the interatomic potential predicts a local minimum (a metastable position) midway in the vacancy migration barrier [14] (see Fig. 2), our choice of  $d_{\text{event}}$  prevents

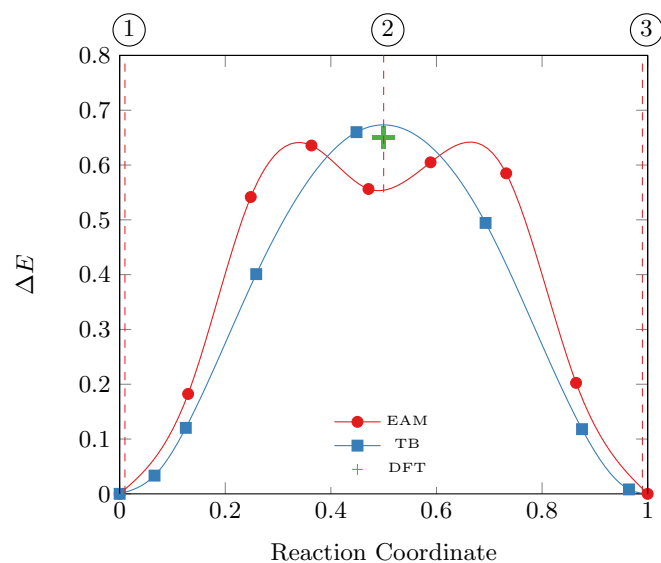


FIG. 2. Minimum energy pathways for the migration of a Fe vacancy in the absence of atomic hydrogen. Results using a EAM potential are presented in red (circles). Results using the TB method are shown in blue (squares). The DFT value is taken from Ref. [16]. The excellent agreement between the TB and DFT activation barriers is not a result of fitting: the TB value is a *prediction* of the theory [21]. The circled numbers indicate each of the configurations presented in Fig. 3 for the EAM potential. The EAM shows an unphysical local minimum at the saddle point; this is a deficiency of the classical model as also observed in Ref. [39].

TABLE III. Effective diffusivity ( $D_{\text{eff}}$ ) of a vacancy in BCC Fe at 800 K. Results are presented for the PRD and MD simulations (the standard deviation is always less than  $2 \times 10^{-12} \text{ m}^2\text{s}^{-1}$ ) and for the analytical model introduced in Sec. III C (using energies calculated both with an EAM potential and with the TB method).

	$D_{\text{eff}}[10^{-11} \text{ m}^2\text{s}^{-1}]$				
			Model		
	PRD	MD	EAM	TB	DFT
0H	9.451	9.073	9.451	7.071	8.175
1H	1.725	2.023	1.974	9.283	
2H	4.685	5.025	3.420	321.562	
3H	6.510	6.567			

the PRD algorithm from counting an event if an atom reaches this metastable position.

Here it is important to mention that for the definition of an event we consider only the motion of the Fe atoms. This will allow us to extract isolated information of the diffusivity of the vacancy, which is the phenomenon of interest.

What this means is that we are ignoring the presence of the H atoms for the definition of the states; it also entails that all the configurations with the same vacancy position (but possibly different H positions) are considered to belong to the same state. Although this is not rigorously correct, we decided to use this assumption based on the fact that the H atoms are much more quickly diffusing than the vacancy, and on the positive results obtained previously in Ref. [32], where systems containing tungsten and helium were studied. To verify the practical validity of our assumption, we compare the results obtained with PRD with standard MD, as shown in Table III. A good agreement between the two methods is obtained.

Finally, for the conjugate gradient minimization algorithm used to check for the occurrence of an event, we use a *normalized* energy tolerance of  $1.0 \times 10^{-5}$  and a force tolerance of  $1.0 \times 10^{-5} \text{ eV}\text{\AA}^{-1}$ .

### 1. Effective diffusivity

The mean-square displacement (MSD) of an atom is a measure of the deviation between its current and its initial position. For a material block consisting of several atoms, the MSD averaged over the number of atoms,  $N$ , can be used to quantify diffusion. The MSD is defined as

$$\text{MSD} = \frac{1}{N} \sum_{i=1}^N |\mathbf{r}_i(t) - \mathbf{r}_i(0)|^2, \quad (2)$$

where  $\mathbf{r}_i(t)$  is a vector containing the coordinates of atom  $i$  at time  $t$ . Once the MSD is known, the diffusivity of the material block can be calculated as

$$D_{\text{sim}} = \frac{\text{MSD}}{6t}. \quad (3)$$

For a material block with a point defect concentration  $x_d$ , the effective diffusivity  $D_{\text{eff}}$  per defect can be computed from

$$D_{\text{eff}} = \frac{D_{\text{sim}}}{x_d}. \quad (4)$$

This effective diffusivity per defect  $D_{\text{eff}}$  is not the same as the “true” diffusivity of the material, since in order to calculate the latter, a system with the equilibrium point-defect concentration is needed [18]. The present work is limited to the calculation of the effective diffusivity of a single vacancy in Fe and the effect that H has on this process.

As previously mentioned, we focus on the diffusion of the vacancy; hence, for the calculation of the MSD we consider only the motion of the Fe atoms.

## 2. Thermal expansion

Diffusion processes are temperature dependent. In order to be able to build simulation cells of appropriate sizes for the PRD simulations, we need to know the equilibrium lattice parameter given by the interatomic potential for bulk body-centered cubic (BCC) Fe as a function of the temperature,  $T$ . For the Fe-Fe part of the current potential [14], the volume per unit cell ( $V$ , in units of  $\text{nm}^3$ ) can be calculated as a function of the temperature (in units of K) using the following interpolation formula, as reported in Ref. [18]:

$$\begin{aligned} V = & 11.64012 + 9.37798 \times 10^{-5} T \\ & + 3.643134 \times 10^{-7} T^2 - 1.851593 \times 10^{-10} T^3 \\ & + 5.669148 \times 10^{-14} T^4. \end{aligned} \quad (5)$$

Note that, for BCC crystals, the lattice parameter,  $a$ , is related to the atomic volume by  $a = (2V)^{1/3}$ .

## 3. System setup

Initially we generate a periodic system containing 250 Fe atoms with a BCC structure; the system has a length of five lattice spacings along each perpendicular direction. The lattice parameter is calculated from Eq. (5) depending on the desired temperature—we vary the temperature from 500 K to 800 K in steps of 100 K. Subsequently we introduce a vacancy to the system by removing one Fe atom, and introduce up to three H atoms in the bulk, outside of the vacancy.

Once the system is generated, we equilibrate it for  $10^5$  time steps, with a time step of  $10^3$  ps (equating to a total of 100 ps) using classical MD and a Langevin thermostat [33,34] (damping factor of 0.1 ps) in a NVE ensemble. During this time, due to their fast diffusion, the H atoms tend to segregate towards the vacancy and remain inside it or in its vicinity.

Finally, after equilibrating the system we proceed to the study of the diffusion of the vacancy using PRD, as previously described in Sec. II C.

## III. RESULTS

### A. Diffusivity via accelerated dynamics

Usually PRD is used to deal with timescales much larger than those attainable with conventional MD. Nevertheless, in the time domain, there is a region where these two methods overlap, and this region can be used to test the soundness of the results. In the present work, we make a comparison between the two methods at a temperature of 800 K.

Two identical systems are set up as described in Sec. II C 3. They are then left to evolve for approximately  $0.2 \mu\text{s}$ , one of them using classical MD and the other one PRD. The

effective diffusivities per defect  $D_{\text{eff}}$  are calculated as previously described in Sec. II C 1 and are presented in Table III. A very good agreement is obtained between both methods, with an average error of 7%. Additionally, the results are consistent with other values reported in the literature [18].

We use PRD to study the evolution in time of a system containing a single vacancy. Although with this method we do not have direct access to the complete dynamic evolution of the system, we do have access to the time and the position of the atoms every time that an event is detected, that is, every time that a vacancy migrates. Since the atomic vibrations of solids are not diffusive we can use the snapshots of the system after each event for the calculation of the MSD (and, subsequently, the diffusivity) without incurring any error. Here it is important to emphasize that we are interested in the diffusivity of only the vacancy and not of the H atoms.

Table II shows the duration of the simulations ( $t_{\text{total}}$ ) which goes up to 20  $\mu\text{s}$ , a time span much larger than the usual timescales that can be reached using MD. To our best knowledge the diffusivity of a vacancy-H complex is calculated at such low temperatures using dynamic simulations with classical potentials previously, and this was possible only due to the use of accelerated dynamic methods (PRD).

Results of the effective diffusivity,  $D_{\text{eff}}$ , of a single vacancy plus zero to three H atoms for different temperatures are presented in Fig. 1 in the form of an Arrhenius plot, showing the logarithm of the diffusion constant versus the inverse of the temperature. The dotted/dashed lines are linear fits to the Arrhenius equation:

$$\ln D_{\text{eff}} = -\frac{\epsilon}{k_B T} + \ln D_0, \quad (6)$$

where  $\epsilon$  is the activation barrier,  $D_0$  is the prefactor,  $T$  is the temperature, and  $k_B$  is the Boltzmann constant. As expected, there is an inverse relation between the two quantities, a clear signature of a single rate-limited thermally activated process. The fits to the Arrhenius equation for the different H concentrations result in the following values for activation barrier: 0.634 eV, 0.752 eV, 0.623 eV, 0.638 eV for the cases of 0H, 1H, 2H, and 3H, respectively.

We note that the addition of one H atom reduces the diffusivity of the vacancy and that, as the amount of H is increased, the diffusivity of the vacancy increases. A more detailed explanation of these phenomena is presented in the following sections.

### B. Energy barriers for vacancy migration

The nudged elastic band (NEB) is a method used to find transition paths between two states by constructing and relaxing a chain of interconnected images. NEB calculations require as input an initial and a final configuration. In the present work, we are interested in the transition paths and energy barriers that a vacancy has to overcome when it migrates along a  $\langle 111 \rangle$  direction to an adjacent position and the influence that atomic H has in such process. For the calculations with the EAM potential, we use the NEB method as implemented in LAMMPS [35–38].

The systems considered for the calculations of the minimum energy paths contain one Fe vacancy (Va) and zero to two H atoms. In general, each of the H atoms can be in only one of two positions, namely, inside or outside the vacancy. In order to facilitate the discussion in the upcoming sections, we introduce the following notation to represent the number of atoms inside ( $n$ ) and outside ( $j$ ) the vacancy for a given system:

$$\text{VaH}_n + j\text{H}.$$

For example, the notation  $\text{VaH}_2 + 1\text{H}$  describes a configuration that contains one vacancy with two H atoms inside and one outside it.

The initial and final atomic configurations for the NEB calculations were chosen to be the relaxed vacancy structures containing up to two H atoms. For the TB approximation nine replicas, i.e., nine atomic configurations connected by springs along the minimum energy pathway, were chosen for the  $\text{VaH}_0$  system and 31 beads for the  $\text{VaH}_1$  and  $\text{VaH}_2$  cases. The initial configurations for the TB NEB calculations were taken from the minimum energy pathway computed using the EAM, which gave a much better approximation to the true minimum energy pathway than a simple interpolation between the initial and final vacancy configurations. The perpendicular force of the spring constants to the minimum energy pathway was then minimized to below  $10^{-3} \text{ eV \AA}^{-1}$ .

For the DFT case, we do not calculate the full minimum energy path due to the prohibitively large computational cost. Instead, we use the climbing image NEB method [36] for finding the maximum energy barriers. The values are drawn using green crosses in Figs. 2, 4, and 5.

#### 1. No hydrogen in the simulation box

In the case where no H is present, the definition of the initial and final configurations is straightforward: one of the Fe atoms adjacent to the vacancy migrates towards the vacancy and fills it, leaving a newly formed vacancy behind (see the case 0H in Fig. 3). There is only one possible initial and final configuration. Using the previously introduced notation, the transition process can be described as follows:



where the asterisk means that the vacancy has hopped to a new position.

Here the initial and final configurations have the same energy, corresponding to global minima of the the system. The transition path of a single vacancy is presented in Fig. 2, where we measure an energy barrier of  $\epsilon_0 = 0.64 \text{ eV}$  (see Table IV), consistent with other values from the literature [14,16].

#### 2. One hydrogen atom in the simulation box

When one H atom is present in the system, it will tend to be trapped by the vacancy and remain inside it.

The migration of a H-vacancy pair in Fe consists of two steps, as shown in case 1H in Fig. 3: first, the H atom hops out of the vacancy to an adjacent position, and, second, the H atom “pushes” one of the neighboring Fe atoms into the vacancy. The moving Fe atom leaves behind a new vacancy that is filled by the H atom, now in a more energetically favorable position.

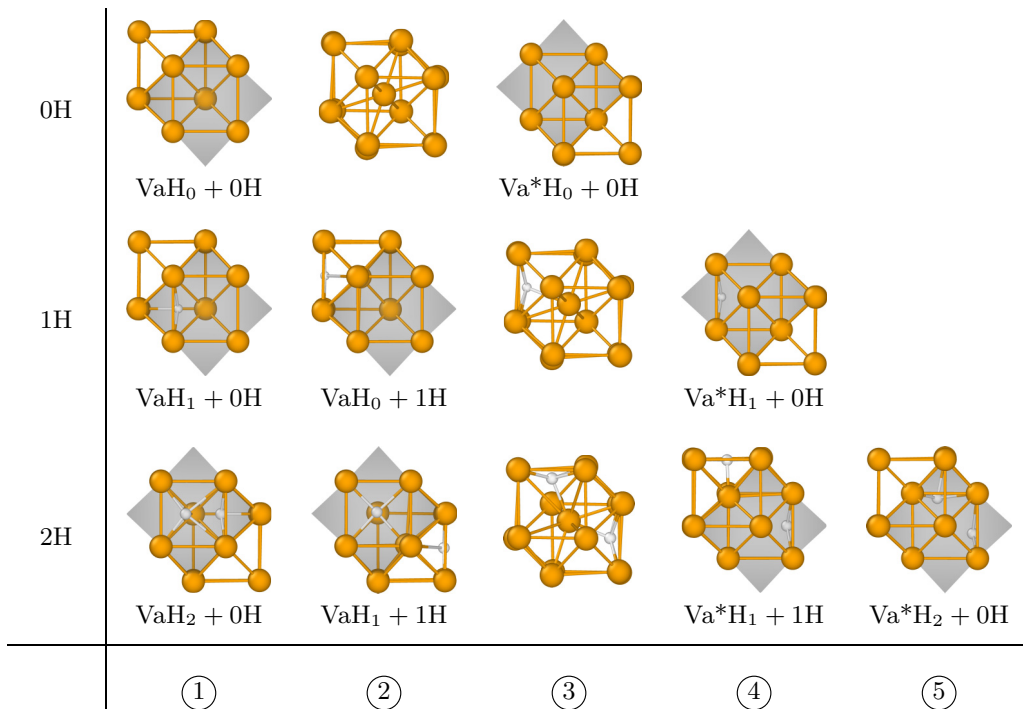
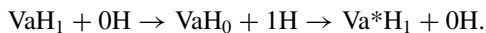


FIG. 3. The process of vacancy migration in the presence of zero, one, and two H atoms following the minimum energy path calculated using the NEB method. The large orange circles represent Fe atoms, while the smaller ones represent H. The vacancy is highlighted by the gray region.

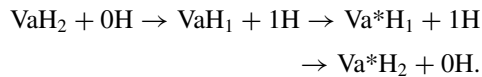
The transition path is not symmetric, as evidenced by the shape of the migration energy barrier (Fig. 4): the energy barrier for the H atom to escape the vacancy (0.597 eV) is lower than that needed for the migration of the vacancy (0.759 eV; see Table IV). This means that, in general, the process of migration will occur in the same direction; that is, the H atom will first escape the vacancy, and, only then, the vacancy will follow. Using our notation convention, we can describe the transition as follows:



### 3. Two hydrogen atoms in the simulation box

For a system containing one vacancy and two H atoms, the transition path is shown in case 2H of Fig. 3. The minimum energy path for the transition calculated using the NEB is presented in Fig. 5. This transition path encompasses two

additional configurations:



The migration of a single Fe vacancy with two H atoms consists of the following steps: first, both H atoms are trapped within the vacancy. Second, one of the H atoms overcomes an energy barrier of 0.369 eV to escape the vacancy and stays in an adjacent position. Third, one of the eight Fe atoms adjacent to the vacancy migrates towards it along a  $\langle 111 \rangle$  direction surpassing an energy barrier of 0.289 eV. The initial vacancy is filled by the Fe atom and a new one is left behind. Similar to the case with one H, one of the H atoms “pushes” the adjacent Fe atom towards the vacancy. Finally, the H atom that remained outside of the newly formed vacancy is attracted to it. The total activation energy for the described migration path is 0.743 eV (see Table IV). We note that there

TABLE IV.  $n$ : Reactant state of the system. For  $n = 1, 2, 3$ , number of H atoms trapped in the vacancy. The subscript 1h represents a system with one H atom inside the vacancy and one in a “helper” position.  $E_n$ : Reference energies as defined in Eq. (10).  $\epsilon_n$ : Activation barriers calculated using the NEB method.  $P_n^{1H}, P_n^{2H}$ : Probability of being in reactant state  $n$  for a system containing a total of one or two H atoms. The units for  $E_n$  and  $\epsilon_n$  are eV.

$n$	EAM				TB			
	$E_n$	$\epsilon_n$	$P_n^{1H}$	$P_n^{2H}$	$E_n$	$\epsilon_n$	$P_n^{1H}$	$P_n^{2H}$
0	0.0	0.640	0.038	0.004	0.0	0.660	0.706	0.547
1	-0.603	0.759	0.962	0.084	-0.319	0.610	0.294	0.209
2	-1.154	0.743		0.912	-0.649	0.548		0.092
1h	-0.454	0.2895		0.001	-0.464	0.269		0.152

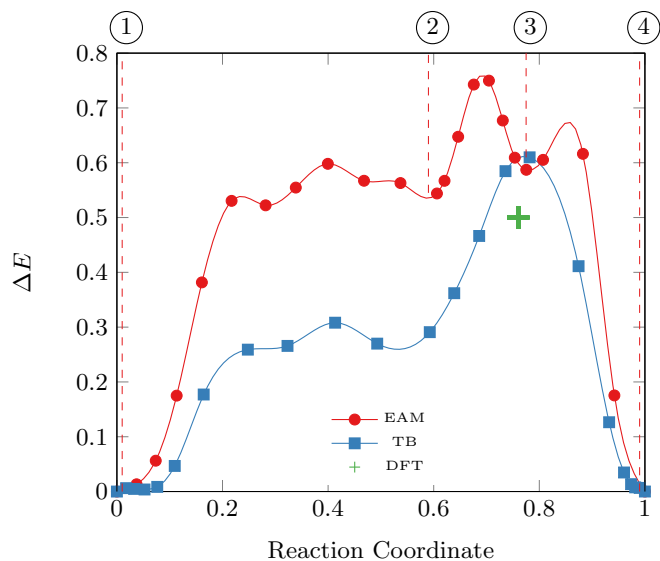


FIG. 4. Minimum energy pathways for the migration of a Fe vacancy with a single H atom. Results using a EAM potential are presented in red (circles). Results using the TB method are shown in blue (squares). The circled numbers indicate the each of the configurations presented in Fig. 3 for the EAM potential. A green cross shows a validating reference calculation using DFT. The identical MEP is found using (essentially) the same EAM in Refs. [11,39].

are different possible configurations of the H atoms inside the vacancy: they can be either on adjacent or in opposite faces; the difference in the migration barriers between the two cases is in the order of 0.05 eV.

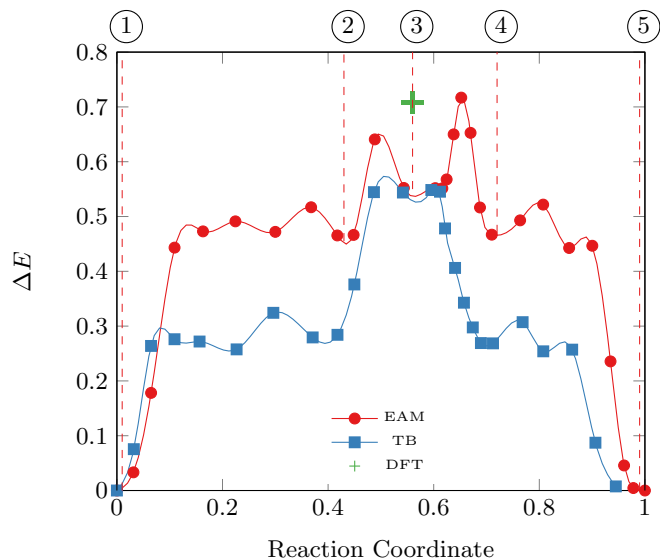


FIG. 5. Minimum energy pathways for the migration of a Fe vacancy with two H atoms. Results using a EAM potential are presented in red (circles). Results using the TB method are shown in blue (squares). The circled numbers indicate the each of the configurations presented in Fig. 3 for the EAM potential. A green cross shows a validating reference calculation of the activation barrier using DFT.

#### 4. General comments

Some general observations can be made about the energetics of the NEB pathways calculated with the various methods. We first highlight an important *qualitative* difference observed in the minimum energy paths as they are predicted by the EAM potential compared with the DFT and TB models. In all cases studied in the present work the EAM potential predicts three critical points in contrast with the TB/DFT models which contain a single critical point. This is a well-known artifact of calculations performed with EAM potentials [35] stemming from artificially sharp truncations in the range of the fitted potential. Although well established, this point is important to emphasise, as it is relevant to the qualitative features of the electronic bonding between the Fe-Fe and Fe-H atom pairs. The DFT and TB calculations, which both permit the formation of bonds and a quantum mechanical redistribution of charge, are both in agreement with respect to the topology of the energy landscape along the minimum energy path with the TB calculations generally predicting a lower potential energy barrier than the DFT calculations. The EAM potential consistently predicts an intermediate minimum in the trajectory. This local minimum occurs when the diffusing Fe atom reaches a midpoint between vacancy sites along a [111] direction and is absent in the two quantum mechanical potentials; this can be seen at the marked points 2, 3, and 3 in the trajectories for the pristine Fig. 2, 1H Fig. 4, and 2H Fig. 5, NEB trajectories.

While the TB and DFT are consistent with respect to the topology of the energy landscape, there are discrepancies with respect to the total energies predicted typically on the order of 0.2 eV. This offset can be traced back to the binding energies of a single H atom to a vacancy predicted by the DFT and TB models. The TB model gives a value 0.3 eV for the binding energy, whereas DFT predicts a binding energy of 0.5 eV [21]. For reference, the experimental value is  $0.4 \pm 0.1$  eV [40].

It is also important to note that the energetics of the reaction pathway are quite sensitive to the lattice constant,  $a$ . Figure 6 demonstrates this dependence for two DFT calculations in the case of a vacancy and a single H atom. The DFT calculations are performed at the relaxed NEB configurations produced by the TB potential and are therefore not the energies for the relaxed DFT NEB pathway.

#### C. Analytical model for diffusion

In this section we set up a very simple model and see where it leads us. More complex models may be envisaged, but here we wish to keep things as simple as possible at the sacrifice of some physics. Refinement of the theory may be left to future work. We consider Table III and note that in the case of pure Fe at 800 K in the PRD simulation we have

$$D = D_0 e^{-\varepsilon_0/k_B T} = 9.451 \times 10^{-11} \text{ m}^2 \text{ s}^{-1}, \quad (7)$$

where, from Fig. 2 and Table IV, we see that  $\varepsilon_0 = 0.64$  eV. We get then that  $D_0 = 1.017 \times 10^{-6} \text{ m}^2 \text{ s}^{-1}$ .

Let us assume that the prefactor  $D_0$  is the same for all concentrations of H. This is reasonable in a zeroth approximation since the attempt frequency in pure iron is dominated by vibrations of the Fe atoms. With the addition of H this cannot be justified, but we adopt this as the simplest model

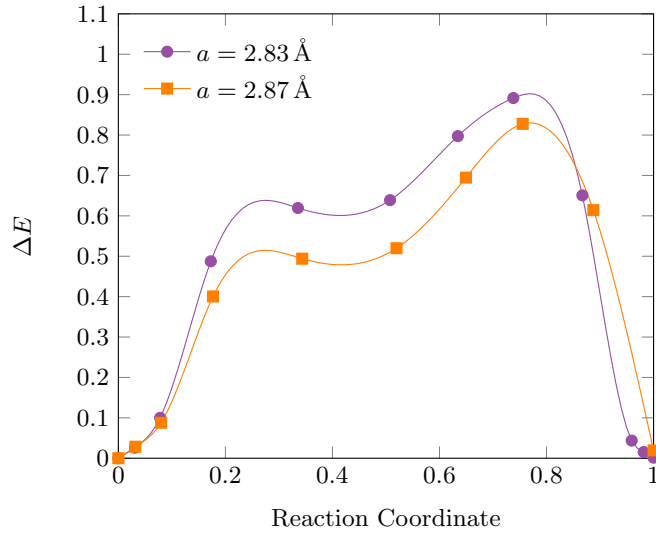


FIG. 6. Variation of the migration energetics calculated using DFT with respect to the lattice constant for the migration of a vacancy in the presence of a single hydrogen atom. The DFT calculations are performed at the relaxed NEB configurations produced by the TB potential and are therefore not the energies for the relaxed DFT NEB pathway.

we may conceive, then its validity may be judged through the predictions of the model.

Note that  $D_0$  includes corrections for the high vacancy concentration, but this is the same in all our simulations. Then, using for the cases 1H and 2H the activation barriers,  $\varepsilon_1$  and  $\varepsilon_2$  shown in Table IV, respectively, we can estimate the diffusivities at 800 K,

$$D_{1H} = D_0 e^{-\varepsilon_1/k_B T} = 1.68 \times 10^{-11} \text{ m}^2 \text{ s}^{-1},$$

$$D_{2H} = D_0 e^{-\varepsilon_2/k_B T} = 2.13 \times 10^{-11} \text{ m}^2 \text{ s}^{-1}.$$

We compare these values to the results of the MD and PRD simulations. The effective diffusivity for 1 H atom is lower than what we find in the simulations. For two H atoms, the calculation underestimates the effective diffusivity. Here, by considering only the migration barriers calculated using NEB, we are ignoring some other possible migration paths for the vacancy. In the following sections we analyze further the migration paths of the vacancy embedded in systems containing one or two H atoms.

### 1. The case of one hydrogen atom

In the case of one H atom, we need to incorporate an additional path for the migration of the vacancy. There are hence two possibilities:

(1) The H-vacancy complex migrates as a coupled system as shown in case 1H of Fig. 3, following the migration path from ① to ④ in Fig. 4.

(2) The H atom is far from the vacancy and the vacancy migrates independently as shown in case 0H of Fig. 3, following the migration path from ① to ③ shown in Fig. 2.

In order to consider several possible paths we construct an effective diffusivity,  $D_{\text{eff}}$ , as follows:

$$D_{\text{eff}} = D_0 \sum P_n e^{-\varepsilon_n/k_B T}, \quad (8)$$

where  $P_n$  is a normalized probability that the system is in a reactant state,  $n$ , defined as follows:

$$P_n = \frac{g_n e^{-E_n/k_B T}}{\sum_m g_m e^{-E_m/k_B T}} = \frac{g_n \mathcal{N}_n}{\mathcal{N}}. \quad (9)$$

These probabilities are proportional to the Boltzmann factor  $e^{-E_n/k_B T}$  times the degeneracy,  $g_n$ , of each configuration of energy  $E_n$  in a system containing  $m$ -H atoms.  $E_n$  is the total energy of  $n$  H atoms trapped in the vacancy and  $(m - n)$  H atoms in solid solution, compared to all  $m$  H atoms being in solution and none trapped in the vacancy, namely,

$$E_n = E_{\text{tot}}[\text{VaH}_n + (m - n)\text{H}] - E_{\text{tot}}[(\text{Va} + m\text{H})]. \quad (10)$$

Calculated values for  $E_n$  are presented in Table IV. The degeneracies  $g_n$  are the number of distinguishable ways of arranging the H atoms for a given configuration. In the case of a single H, this is the number of ways (six) of arranging the H atom on the octahedral site at the six faces of a vacancy ( $g_0$ ), and the number of ways of arranging the unbound atom in the ( $N_T - 24$ ) available tetrahedral sites in the system ( $g_1$ ):

$$g_0 = 6,$$

$$g_1 = (N_T - 24).$$

Combining these degeneracies ( $g_0$  and  $g_1$ ) with the corresponding migration barriers ( $\varepsilon_0$  and  $\varepsilon_1$ ) and reference energies ( $E_0$  and  $E_1$ ) (see Table IV), we can calculate the effective diffusivity. We obtain  $D_{1H} = 1.974 \times 10^{-11} \text{ m}^2 \text{ s}^{-1}$ , in agreement with the results obtained in the PRD and MD simulations (see Table III and Fig. 1).

### 2. The case of two H atoms

In the case of two H atoms we note that there is a *further possible process* with a very low activation barrier of  $\varepsilon_{1h} = 0.2895 \text{ eV}$  (see Fig. 5) from configuration ② to ⑤. It corresponds to the energy barrier to pass from  $\text{VaH}_1 + 1\text{H}$  to  $\text{Va}^*\text{H}_2 + 0\text{H}$  (see case 2H in Fig. 3).

This lower energy barrier corresponds to a configuration in which one H atom is trapped inside the vacancy, and one additional H atom is located adjacent to it. We will call this additional atom a “helper” atom because it facilitates the migration of the vacancy. Note that for a H atom to be considered a helper it needs to be accompanied by (at least) a second H atom trapped in the vacancy. If a single unaccompanied H atom finds itself adjacent to the vacancy, it will become trapped on a much shorter timescale than the vacancy jump time.

How many helper sites are there? On the timescale of Fe jumping (roughly 1 ps) we know that the H samples all six octahedral sites, and indeed most of the environment close to them. In fact, the H is in a proton delocalized wave function; see Cheng *et al.* [41].

Since the vacancy jump is along a  $\langle 111 \rangle$  direction, there are eight Fe atoms that may fill in the former vacant position after the vacancy jump. A H atom is considered to be a “helper”

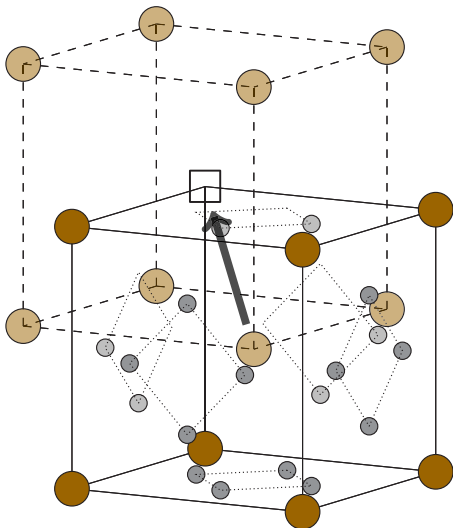


FIG. 7. Route for a Fe atom to fill in a vacancy (depicted as a white square) along a  $(111)$  direction in the event of a vacancy jump. The potential tetrahedral positions for a “helper” H atom are shown (small gray and light gray circles). For clarity only one of the eight surrounding unitcells is drawn. A total of  $N_h = 120$  potential tetrahedral positions for “helper” atoms are available per vacancy.

when it is located next to one of the eight Fe atoms that surround the vacancy.

How many helper sites are associated with each? (See Fig. 7.) We might think of the helper atoms as “pushing” their associated Fe atom into the vacant site. They do this because once the Fe atom has left they are now bound to a vacancy and have gained about 0.6 eV. However, the H atom inside the vacancy is “repelling” the Fe atom because it will lose 0.6 eV when it is no longer bound to a vacancy; this is why in the final stage it will jump into the vacancy and join the helper. To find the number of helper sites we count all of the tetrahedral sites in the cube having darker shade atoms in Fig. 7 that are *not* in the vacancy. On three faces there are four sites (dark gray circles), and on the other three there are two sites (light gray circles). But these second three sites are *shared* by two of the eight Fe atoms. Hence, we have  $N_h = (3 \times 4 + (3 \times 2)/2) \times 8 = 120$  sites.

If we consider the additional possibility of a “helper” atom paired with another H atom sitting inside a vacancy in a system that contains one vacancy and two hydrogen atoms, there are the following four possibilities for vacancy migration:

(1) The H-H-vacancy complex migrates as a coupled system as shown in case 2H of Fig. 3 following the migration path of Fig. 5.

(2) One of the H atoms is far from the vacancy and the other one is inside of the vacancy. The H-vacancy complex migrates as a coupled system as shown in case 1H of Fig. 3 following the migration path of Fig. 4.

(3) The two H atoms are far from the vacancy and the vacancy migrates independently as shown in case 0H of Fig. 3 following the migration path shown in Fig. 2.

(4) One of the H atoms is adjacent to the vacancy in one of the  $N_h = 120$  positions suitable for the atom to be consider a “helper.” The other H atom is in the vacancy. The vacancy

migrates from configuration  $VaH_1 + 1H$  to  $Va^*H_1 + 1H$ , as shown in case 2H of Fig. 3.

For the previously mentioned four possibilities, we have the following degeneracies:

$$\begin{aligned} g_2 &= 6 \times 5, \\ g_1 &= 24 \times (N_T - 24 - N_h), \\ g_0 &= (N_T - 24) \times (N_T - 24 - 1), \\ g_{1h} &= 6 \times N_h, \end{aligned}$$

where  $g_2$  allows for six octahedral sites for the first H and five possibilities for the second H in the vacancy.  $g_1$  allows for the total number of tetrahedral sites,  $N_T$ , being reduced by 24 inside the vacancy plus the number of possible sites for the helper atom.  $g_0$  is the number of sites available to “outside” H atoms.  $g_{1h}$  is the degeneracy in the case that there is one H in the vacancy and one in a helper position.

For the case of the “helper” H atom we calculate a barrier of  $\varepsilon_{1h} = 0.2895$  eV in the EAM and a reference energy of  $E_{1h} = -0.454$  eV. Reading the values of  $\varepsilon_0$ ,  $\varepsilon_1$ ,  $\varepsilon_2$ , and  $E_0$ ,  $E_1$ , and  $E_2$ , we can calculate the effective diffusivity using Eq. (8). This results in  $D_{2H} = 3.420 \times 10^{-11} \text{ m}^2\text{s}^{-1}$ , in agreement with the results obtained in the PRD and MD simulations (see Table III and Fig. 1).

## IV. DISCUSSION

### A. Application of the analytical model

So far, we have demonstrated two principal findings. First, we have proposed an analytical model for the calculation of the diffusivity of vacancies in the presence of H atoms, and we have validated it for the case of classical MD using a EAM potential. Second, we have calculated minimum energy paths for the migration of vacancies (with and without H) using the TB method and demonstrated their accuracy by comparing the migration barrier with DFT calculations using the climbing image NEB. We now proceed to apply our analytical model to the more accurate migration and reference energies calculated using the TB method.

As previously done with the EAM potentials, we take the same value for the prefactor  $D_0$ . For the calculation of the diffusivities in systems containing a vacancy and one or two H atoms, we use Eqs. (8) and (9) with the same degeneracies used for the EAM case, and the reference energies and energy barriers calculated with tight binding (see Table IV). The results are presented in Table III and Fig. 1.

For the case of a system containing one H atom, there is a considerable difference in the effective diffusivity,  $D_{\text{eff}}$ , between the model calculations performed with the EAM and TB energies ( $1.974$  vs  $9.283 \times 10^{-11} \text{ m}^2\text{s}^{-1}$ ; see Table III and Fig. 1). The reason is that in the case of EAM the process is dominated by the configuration where the H atom is far from the vacancy, with a transition energy of 0.640 eV, while in the case of TB the process is dominated by the configuration where one H atom is in the vacancy, with a lower energy barrier of 0.610 eV. The probabilities of being in a given reactant state, calculated using Eq. (9), are presented in Table IV.

For the case with a vacancy and two H atoms, we also get a considerable increase of  $D_{\text{eff}}$  when comparing the results of

the model using the TB and EAM energies (3.420 vs 321.562  $10^{-11} \text{ m}^2\text{s}^{-1}$ ; see Table III and Fig. 1). The discrepancy between the values is due to the difference in probabilities of being in a given reactant state; see column  $P_n^{2H}$  in Table IV. When using EAM, there is a clear preference for the system to remain in reactant state  $\text{VaH}_2 + 0\text{H}$  because the reference energy of such a state is much lower than that of the others ( $E_2 < E_1 < E_{1h} < E_0$ ). In contrast, when using TB, while the dominant state is  $\text{VaH}_0 + 2\text{H}$ , the contributions of the other states remain significant. This is especially significant for the state  $\text{VaH}_1 + 1\text{Hh}$  (one atom in the vacancy and one helper atom), which has a lower migration barrier that can accelerate the diffusion process.

It is discouraging that there is as much as a two orders of magnitude discrepancy between the EAM and the TB diffusivities. But it must be remembered that the outcomes are dominated by energy barriers that appear as the argument to an exponential. Any activated process is highly sensitive to its activation barriers. The EAM is fitted to the energy barrier in pure Fe and also to the binding energy of H to the vacancy. These are not fitted in the TB model, and so TB appears at a disadvantage. However, we expect the TB to be more reliable in cases such as 2H (Fig. 5) since the model is based in quantum mechanics. Therefore we expect the TB results in Table III and Fig. 1 to be the more reliable. On the other hand PRD and MD on the timescales reachable by the EAM are outside the reach of TB, not to mention DFT. Therefore the value of the present work has to be evaluated in this context. The EAM is essential in allowing the diffusivity to be calculated in a way that accounts properly for geometry factors, anharmonicity, and probability factors. We have used the data to map the EAM results to an analytic model that depends only on energy barriers that can be calculated in DFT. The large-scale NEB calculations are still out of reach of DFT. The value of the analytic model is that it offers insight into the atomic processes, for example, the “helpers,” that lie behind the enhancement or attenuation of vacancy diffusivity due to hydrogen.

The DFT and TB outcomes are generally in accord with each other. The principal variance is due to differences in the calculated trap energies of one hydrogen atom by the vacancy. As is evident from Table I and the shoulder in Fig. 4 the energy barrier to trap a hydrogen atom in a vacancy using TB is about 0.32 eV [41,42], while the EAM trap energy is fitted to the DFT value of about 0.6 eV. On the other hand the use of a quantum mechanical calculation and its employment in our analytical model allows us to avoid the conclusion in Table III and Fig. 1 from the MD and PRD simulations that the diffusivity is at first attenuated and then enhanced as the concentration of hydrogen is increased. On the contrary the analytic model based on the TB minimum energy paths predicts that the diffusivity increases monotonically with hydrogen concentration. We believe that the quantum mechanical TB approximation, rather than the classical potential, better represents the reality.

One of our principal assertions here is that the self diffusivity in  $\alpha$ -Fe increases monotonically with hydrogen concentration—a result not obtained in the classical EAM potential, but recovered by the inclusion of quantum mechanics in the description of interatomic forces. This has a significant bearing on some recent experimental and theoretical

findings. Neeraj and Srinivasan [43,44] have found evidence of nanovoids at fracture surfaces in some X-series pipe grade steels. This has raised the important question of whether dislocation activity coupled to enhanced vacancy concentration and diffusivity can serve to cause vacancy-hydrogen complexes to coalesce into hydrogen-filled nanovoids. This may be regarded as a mechanism for hydrogen embrittlement [39,45]. Because in these two papers [39,45] a classical EAM potential was used in their simulations, there is reason to believe that conclusions may be misleading at that level of theory.

Based on our results, we may propose a similar mechanism to that suggested by Tehranchi *et al.* [45]. It is known that nanovoids are present at intergranular fracture surfaces; it is then possible that the higher diffusivity of the VaH complex that we predict allows for its faster diffusion to grain boundaries. Once there, they can progressively accumulate and form the voids that have been experimentally observed.

## V. CONCLUSIONS

In the present article simulations of vacancy diffusion and the effect that hydrogen has on this process were performed using parallel replica dynamics (PRD), the nudged-elastic-band (NEB) method, and an analytical model based on the minimum energy paths of migration.

PRD allowed us to calculate the diffusivity of a single vacancy and the influence that atomic H has on vacancy migration for temperature/timescale combinations that are currently not reachable using classical MD. Our results showed that PRD can also be used for systems in which more than one type of infrequent-event phenomenon occurs, namely, vacancy migration and hydrogen diffusion.

Using NEB calculations of the minimum energy path of migration of vacancy-H complexes and a visual inspection of the trajectories of the H atom(s) during the PRD simulations, we identified a mechanism for the migration of vacancy-H complexes. When at least one H atom is trapped inside the vacancy, and one additional H atom is located adjacent to it, the migration barriers are considerably reduced. We called this additional H atom a “helper” atom because it facilitates the migration of the vacancy.

Finally, based on the NEB calculations we propose an analytical model to calculate the diffusivity of a single vacancy surrounded by H atoms. The model is based on the fact that the diffusivity of a vacancy-H complex is dependent not only on a single migration barrier, but also on the degeneracies of the initial and final configurations and their corresponding migration paths.

## ACKNOWLEDGMENTS

S.E.R. would like to thank W. A. Curtin and A. Tehranchi for enlightening discussions and for sharing the files for the EAM interatomic potential. S.E.R. would also like to thank Predrag Andric for his critical review of the final manuscript. A.T.P. and H.L. are supported by EPSRC under the HEMs Programme Grant EP/L014742. This work was supported in part through the computational resources and staff contributions provided for the Comlab high-performance computing facility at SKF Research & Technology Development, Houten, the Netherlands.

- [1] R. A. Oriani, *Annu. Rev. Mater. Sci.* **8**, 327 (1978).
- [2] I. H. Katzarov, D. L. Pashov, and A. T. Paxton, *Phys. Rev. Mater.* **1**, 033602 (2017).
- [3] I. H. Katzarov and A. T. Paxton, *Phys. Rev. Mater.* **1**, 033603 (2017).
- [4] H. Bhadeshia, *Prog. Mater. Sci.* **57**, 268 (2012).
- [5] F. Caballero, H. Bhadeshia, K. Mawella, D. Jones, and P. Brown, *Mater. Sci. Technol.* **17**, 512 (2001).
- [6] D. Raabe, D. Ponge, O. Dmitrieva, and B. Sander, *Adv. Eng. Mater.* **11**, 547 (2009).
- [7] L. W. Tsay and T. Y. Yang, *Fatigue Fract. Eng. Mater. Struct.* **23**, 325 (2000).
- [8] D. Figueroa and M. Robinson, *Corros. Sci.* **50**, 1066 (2008).
- [9] H. K. D. H. Bhadeshia, *ISIJ Int.* **56**, 24 (2016).
- [10] Q. Xu and J. Zhang, *Sci. Rep.* **7**, 16927 (2017).
- [11] E. Hayward and C. C. Fu, *Phys. Rev. B* **87**, 174103 (2013).
- [12] A. Ramasubramaniam, M. Itakura, and E. A. Carter, *Phys. Rev. B* **79**, 174101 (2009).
- [13] J. Song and W. A. Curtin, *Nat. Mater.* **12**, 145 (2012).
- [14] G. J. Ackland, M. I. Mendeleev, D. J. Srolovitz, S. Han, and A. V. Barashev, *J. Phys.: Condens. Matter* **16**, S2629 (2004).
- [15] M. S. Daw and M. I. Baskes, *Phys. Rev. B* **29**, 6443 (1984).
- [16] C. Domain and C. S. Becquart, *Phys. Rev. B* **65**, 024103 (2001).
- [17] M. I. Mendeleev, S. Han, D. J. Srolovitz, G. J. Ackland, D. Y. Sun, and M. Asta, *Philos. Mag.* **83**, 3977 (2003).
- [18] M. I. Mendeleev and Y. Mishin, *Phys. Rev. B* **80**, 144111 (2009).
- [19] Y. Tateyama and T. Ohno, *Phys. Rev. B* **67**, 174105 (2003).
- [20] D. Mirzaev, A. Mirzoev, K. Okishev, and A. Verkhoviykh, *Mol. Phys.* **112**, 1745 (2014).
- [21] A. T. Paxton and C. Elsässer, *Phys. Rev. B* **87**, 224110 (2013).
- [22] A. Paxton, *Multiscale Simulation Methods in Molecular Sciences*, NIC Series Vol. 42 (Jülich Supercomputing Centre, Forschungszentrum Jülich, 2009), pp. 145–174.
- [23] <https://www.questaal.org>.
- [24] V. Kapil, M. Rossi, O. Marsalek, R. Petraglia, Y. Litman, T. Spura, B. Cheng, A. Cuzzocrea, R. H. Meiner, D. M. Wilkins, *et al.*, *Comput. Phys. Commun.* **236**, 214 (2019).
- [25] G. Kresse and J. Furthmüller, *Phys. Rev. B* **54**, 11169 (1996).
- [26] J. P. Perdew, K. Burke, and M. Ernzerhof, *Phys. Rev. Lett.* **77**, 3865 (1996).
- [27] P. E. Blöchl, *Phys. Rev. B* **50**, 17953 (1994).
- [28] A. F. Voter, *Phys. Rev. B* **57**, R13985 (1998).
- [29] A. F. Voter, F. Montalenti, and T. C. Germann, *Annu. Rev. Mater. Res.* **32**, 321 (2002).
- [30] S. Plimpton, *J. Comput. Phys.* **117**, 1 (1995).
- [31] <http://lammps.sandia.gov>.
- [32] D. Perez, L. Sandoval, S. Blondel, B. D. Wirth, B. P. Uberuaga, and A. F. Voter, *Sci. Rep.* **7**, 2522 (2017).
- [33] T. Schneider and E. Stoll, *Phys. Rev. B* **17**, 1302 (1978).
- [34] B. Dünweg and W. Paul, *Int. J. Mod. Phys. C* **02**, 817 (1991).
- [35] G. Henkelman and H. Jónsson, *J. Chem. Phys.* **113**, 9978 (2000).
- [36] G. Henkelman, B. P. Uberuaga, and H. Jónsson, *J. Chem. Phys.* **113**, 9901 (2000).
- [37] A. Nakano, *Comput. Phys. Commun.* **178**, 280 (2008).
- [38] E. Maras, O. Trushin, A. Stukowski, T. Ala-Nissila, and H. Jónsson, *Comput. Phys. Commun.* **205**, 13 (2016).
- [39] S. Li, Y. Li, Y.-C. Lo, T. Neeraj, R. Srinivasan, X. Ding, J. Sun, L. Qi, P. Gumbsch, and J. Li, *Int. J. Plast.* **74**, 175 (2015).
- [40] S. M. Myers, S. T. Picraux, and R. E. Stoltz, *J. Appl. Phys.* **50**, 5710 (1979).
- [41] B. Cheng, A. T. Paxton, and M. Ceriotti, *Phys. Rev. Lett.* **120**, 225901 (2018).
- [42] A. T. Paxton, *Mater. Sci. Technol.* **30**, 1063 (2014).
- [43] T. Neeraj, R. Srinivasan, and J. Li, *Acta Mater.* **60**, 5160 (2012).
- [44] T. Neeraj and R. Srinivasan, *Corrosion* **73**, 437 (2017).
- [45] A. Tehranchi, X. Zhang, G. Lu, and W. A. Curtin, *Modell. Simul. Mater. Sci. Eng.* **25**, 025001 (2017).